Ocean Science Journal, *Vol. 41 No. 4, 235-244(2006)*

Article

Ocean Science Journal

http://osj.kordi.re.kr

Estimation of the PAR Irradiance Ratio and Its Variability under Clear-sky Conditions at Ieodo in the East China Sea

Do-Seong Byun[1]* and Yang-Ki Cho[2]

[1]*Ocean Research Laboratory, National Oceanographic Research Institute, Incheon 400-800, Korea*

[2]*Department of Oceanography, College of Natural Sciences, Chonnam National University, Gwangju 500-757, Korea*

Received 11 September 2006; Revised 15 December 2006; Accepted 22 December 2006

Abstract – Determining 'photosynthetically active radiation' (PAR) is a key part of calculating phytoplankton productivity in a biogeochemical model. We explore the daily and seasonal variability in the ratio of PAR irradiance to total irradiance that occurred at Ieodo Ocean Research Station (IORS) in the East China Sea under clear-sky conditions in 2004 using a simple radiative transfer model (RTM). Meteorological data observed at IORS and aerosol optical properties derived from Aerosol Robotic Network observations at Gosan are used for the RTM. Preliminary results suggest that the use of simple PAR irradiance-ratio values is appropriate in calculating phytoplankton productivity as follows: an average of 0.44 (±0.01) in January to an average of 0.48 (±0.01) in July, with average daily variabilities over these periods of about 0.016 (±0.008) and 0.025 (±0.008), respectively. The model experiments demonstrate that variations in the major controlling input parameters (i.e. solar zenith angle, precipitable water vapor and aerosol optical thickness) cause PAR irradiance ratio variation at daily and seasonal timescales. Further, increases (>0.012) in the PAR irradiance ratio just below the sea-surface are positively correlated with high solar zenith angles and strong wind stresses relative to those just above the sea-surface.

Key words – PAR, irradiance, radiative transfer model, ecosystem model, East China Sea, Ieodo

1. Introduction

Rates of phytoplankton photosynthesis are proportional to the number of available photons, rather than to the total amount of radiant energy. Photosynthetically active radiation (PAR, quanta m^{-2} s^{-1}), comprising the useful wavebands for phytoplankton photosynthesis, is defined as the total photon flux at 350-700 nm (practically, 400-700 nm):

$$PAR = \int_{350}^{700} \frac{\lambda}{hc} E_d(\lambda) d\lambda \quad (1)$$

where h (=6.6255×10^{-34} J s) is Planck's constant and c (=2.998×10^{17} nm s^{-1}) is the speed of light, E_d (W m^{-2} nm^{-1}) is global downwelling irradiance and λ (nm) is wavelength.

As shown in Eq. (1), the monochromatic E_d is converted into quantum units according to $\frac{\lambda}{hc}$, whereas the total irradiance from 350 to 700 nm cannot be directly converted into quantum units due to their wavelength dependence. Morel and Smith (1974) revealed the linear relationship between PAR quanta and the integrated irradiance from 350 to 700 nm (PAR irradiance, E_{PAR}) based on observations from 300-2800 nm. That is, the average ratio of PAR quanta to E_{PAR} is 2.72×10^{18} (±0.02) quanta s^{-1} W^{-1}. This relationship can be used to estimate the amount of PAR from the given E_{PAR}. Further, PAR can be estimated from total downwelling irradiance (E_D) across the entire spectral domain if the ratio of E_{PAR} to E_D (hereafter, conversion factor F_c) is known or can be predicted. That is, F_c is calculated by:

$$F_c = \frac{E_{PAR}}{E_D} \quad (2a)$$

$$E_{PAR} = \int_{350}^{700} E_d(\lambda) d\lambda \quad (2b)$$

$$\text{and } E_D = \int_{200}^{4000} E_d(\lambda) d\lambda \quad (2c)$$

*Corresponding author. E-mail: dsbyun@nori.go.kr

In biogeochemical models or calculations of phytoplankton production, PAR is commonly parameterized by multiplying a constant F_c value by the average ratio of PAR quanta to E_{PAR} by E_D (i.e. PAR=$2.72\times10^{18}\cdot E_{PAR}$=$2.72\times10^{18}\cdot F_c\cdot E_D$). Conventionally F_c is assumed to equal half the total incoming irradiance (*e.g.* Parsons *et al.* 1984; Ebenhöh *et al.* 1997; Baretta-Bekker *et al.* 1997; Colijn and Cadée *et al.* 2003). Several studies, however, have used or reported different F_c values: 0.40 by Zavatarelli *et al.* (2000), 0.43 by Jitts *et al.* (1976) and Morel (1988), 0.46 by Tilzer and Goldman (1978) and Byun *et al.* (2005), and 0.49 by Knauss (1997). In fact, at the top of the atmosphere, PAR irradiance accounts for an almost constant 43% of total irradiance, while the ratio varies throughout the atmosphere according to atmospheric and geometrical conditions (Baker and Frouin 1987; Jacovides *et al.* 2003). In ecosystem model simulations with three different PAR fractions (*i.e.* 0.43, 0.46 and 0.49), Byun *et al.* (2006) showed that the development of phytoplankton spring blooms is significantly affected by different PAR fraction values. This finding provides the impetus for the present investigation into actual variation in the PAR fraction.

In this paper we take a step back from ecosystem model simulations in the East China Sea to investigate daily and seasonal variability in the ratio of E_{PAR} to E_D, just above and below the sea-surface under clear-sky conditions using a simple clear-sky maritime spectral radiative transfer model (RTM). Field data provided from the IORS (Ieodo Ocean Research Station) make it possible to examine for the first time daily and seasonal F_c variability in the East China Sea. Further, we investigate the main meteorological and atmospheric parameters controlling variation in F_c through model sensitivity simulations exploring the effect of each input parameter on the PAR fraction.

2. Radiative Transfer Model description

The RTM used in this work includes the entire solar spectra (200-4000 nm), with a relatively fine resolution (25 nm) in the PAR (350-700 nm) range and relatively coarse resolutions (from 50 to 800 nm) in the other spectral ranges. This model is primarily based on Gregg (2002) and Gregg and Carder (1990)'s clear-sky maritime spectral-irradiance model.

The total downwelling irradiance in the RTM comprises the sum of two irradiance components, the spectral-direct ($E_{dd}(\lambda, 0^+)$) and diffuse (E_{ds} (λ, 0^+)) downwelling irradiances. That is, the global downwelling irradiance just above the sea-surface, E_d (λ, 0^+), is expressed by:

$$E_d(\lambda, 0^+) = E_{dd}(\lambda, 0^+) + E_{ds}(\lambda, 0^+) \quad (3)$$

where 0^+ represents a level above the sea-surface. The direct downwelling and diffuse irradiances arriving just above the sea surface are calculated by atmospheric spectral attenuation processes according to solar zenith angle variation, and are expressed as (Gregg 2002):

$$E_{dd}(\lambda, 0^+) = \frac{Q_0(\lambda)}{r^2}\cos\theta Tr_r(\lambda)Tr_{oz}(\lambda)Tr_{o_2}(\lambda)Tr_{co_2}(\lambda)Tr_w(\lambda) \quad (4)$$

$$E_{ds}(\lambda, 0^+) = E_r(\lambda) + E_a(\lambda) \quad (5a)$$

$$E_r(\lambda) = \frac{1}{2}\frac{Q_0(\lambda)}{r^2}\cos\theta Tr_{oz}(\lambda)Tr_{o_2}(\lambda)Tr_{co_2}(\lambda)Tr_w(\lambda)Tr_{aa}(\lambda)(1-Tr(\lambda)_r^{0.95}) \quad (5b)$$

and

$$E_a(\lambda) = \frac{Q_0(\lambda)}{r^2}\cos\theta Tr_{oz}(\lambda)Tr_{o_2}(\lambda)Tr_{co_2}(\lambda)Tr_w(\lambda)Tr_{aa}(\lambda)Tr(\lambda)_r^{1.5}(1-Tr_{as}(\lambda))F_a(\theta) \quad (5c)$$

where $Q_0(\lambda)$ is the spectral mean extraterrestrial solar irradiance, r is Sun-Earth radius vector, θ is the solar zenith angle, $Tr(\lambda)$ is the atmospheric transmittance of each spectrum after absorption and scattering (*i.e.* Tr_r after aerosol scattering, Tr_a after aerosol scattering and absorption, Tr_{oz}, Tr_{o2}, Tr_{co2} and Tr_w after ozone, oxygen, carbon dioxide, and water-vapor absorptions respectively, Tr_{aa} after aerosol absorption alone, and Tr_{as} after aerosol scattering alone) and F_a is the forward scattering probability of the aerosol. The parameterizations of each transmittance used are referenced in Table 1.

Direct and diffuse sea-surface reflectances depend on the sea-surface roughness and whitecaps (and sea foam) produced by vigorous breaking waves (Koepke 1984;

Table 1. Parameterizations of each atmospheric transmittance after absorption and scattering in the RTM

Transmittance	Attenuation coefficient	Reference
$T_r(\lambda) = \exp\left[-\frac{p^*}{p_0^{**}}M(\theta)\tau_r(\lambda)\right]$	M(θ): atmospheric path length $\tau_r(\lambda)$: Rayleigh scattering	Kasten and Young (1989) Gueymard (2001)
$T_{oz}(\lambda) = \exp[-M_{oz}(\theta)H_{oz}a_{oz}(\lambda)]$	$M_{oz}(\theta)$: ozone path length H_{oz}: ozone scale height $a_{oz}(\lambda)$: ozone absorption	Paltridge and Platt (1976) Van Heuklon (1979) Gregg (2002)
$T_0(\lambda) = \exp\left[\frac{-1.41a_0(\lambda)M(\theta)}{\{1+11.83a_0(\lambda)M(\theta)\}^{0.45}}\frac{p^*}{p_0^{**}}\right]$	$a_o(\theta)$: oxygen and carbon dioxide absorption	Gregg (2002)
$T_w(\lambda) = \exp\left[\frac{-0.2385a_w(\lambda)P_{wv}M(\theta)}{\{1+20.07a_w(\lambda)P_{wv}M(\theta)\}^{0.45}}\right]$	$a_w(\lambda)$: water vapor absorption P_{wv}: precipitable water vapor	Gregg (2002) Gueymard (1994)
$T_a(\lambda) = \exp[-M(\theta)\tau_a(\lambda)]$	$\tau_a(\lambda)$: aerosol optical thickness	Gosan AERONET
$T_{aa}(\lambda) = \exp[-(1-\omega_a)M(\theta)\tau_a(\lambda)]$ $T_{as}(\lambda) = \exp[-\omega_a M(\theta)\tau_a(\lambda)]$	$\omega_a(\lambda) = f(\mathrm{AM}, R_H)$: single-scattering aerosol albedo	Justus and Paris (1985); Gregg (2002)

*P is atmospheric pressure and **P_0 is standard pressure (1013.25 hPa).

Stramska and Petelski 2003). The direct surface reflectance (R_d) and diffuse surface reflectance (R_s) components of the RTM comprise the sum of the specular reflectances (R_{dsp} and R_{ssp}) and foam reflectance (R_f). The specular reflectance components are parameterized as a function of wind speed and solar zenith angle for R_{dsp}, and of wind speed alone for R_{ssp} (Gregg and Carder, 1990). Foam reflectance components are parameterized as functions of wind speed and an adjusting factor for foam reflectance (Gregg 2002). Applying these parameterizations to Eq. (4) and (5a), direct and diffuse downwelling irradiances just below the sea-surface may be expressed as (Gregg 2002):

$$E_{dd}(\lambda, 0^-) = E_{dd}(\lambda, 0^+)[1 - R_d(W_{sp}, \lambda)] \quad (6a)$$

$$R_d(W_{sp}, \lambda) = R_{dsp}(W_{sp}, \theta) + R_f(W_{sp})F(\lambda) \quad (6b)$$

and

$$E_{ds}(\lambda, 0^-) = [E_r(\lambda) + E_a(\lambda)][1 - R_s(W_{sp}, \lambda)] \quad (7a)$$

$$R_s(W_{sp}, \lambda) = R_{ssp}(W_{sp}, \theta) + R_f(W_{sp})F(\lambda) \quad (7b)$$

where 0^- represents a level just below the sea-surface, W_{sp} is wind speed and F is an adjustment factor for spectral foam reflectance.

3. Description of RTM input data

The RTM for clear-sky conditions requires meteorological input data (*i.e.* total precipitable water vapor (P_{wv}), relative humidity (RH), air temperature (T_{air}), atmospheric pressure (A_p) and wind speed (W_{sp})) and atmospheric condition data (*i.e.* air-mass type (AM) and aerosol optical properties). The IORS, which is situated on submarine rock off the typical-oceanic island of Ieo (Ieodo) in the East China Sea (Fig. 1), has measured offshore meteorological and oceanographic data since June 2003 (Shim *et al.* 2004). Hourly meteorological observations (RH, T_{air}, A_p, W_{sp}) from IORS in 2004 (Fig. 2) were provided by the KORDI (Korea Ocean Research and Development Institute). These

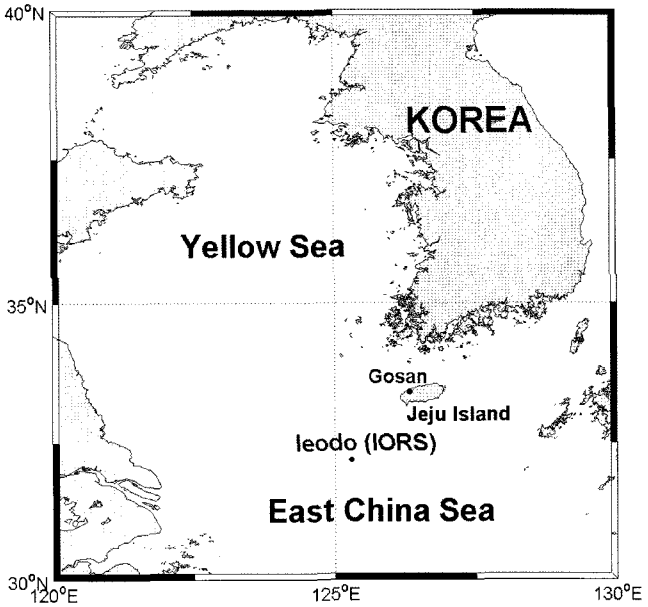

Fig. 1. Location of the Ieodo Ocean Research Station (IORS) and Gosan, Jeju Island.

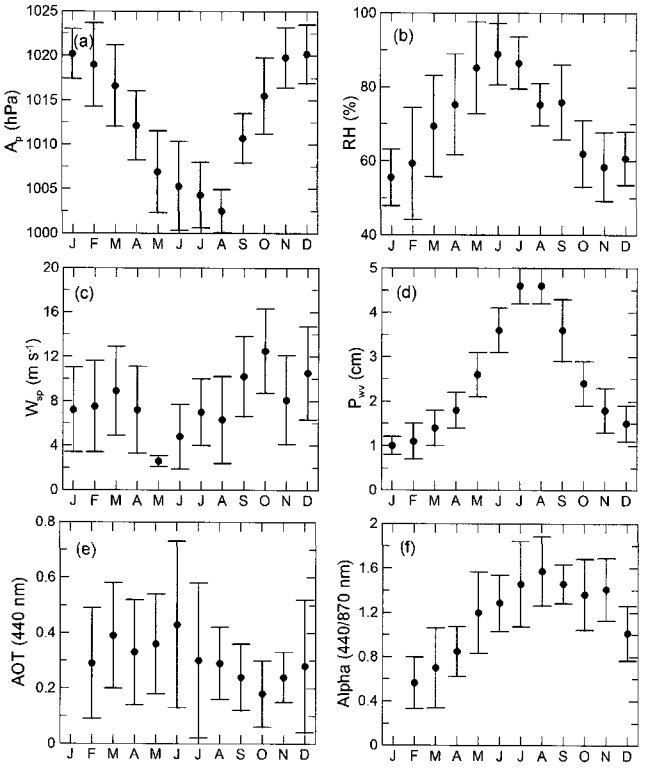

Fig. 2. Monthly variability in the main meteorological parameters ((a) air pressure (A_p), (b) relative humidity (RH), (c) wind speed (W_{sp}) and (d) precipitable water vapor (P_{WV})) at the IORS, and aerosol optical properties ((e) aerosol optical thickness (440nm, AOT) and (f) Ångström exponent (α)) at Gosan derived from AERONET Level 2 data in 2004.

data are used as direct RTM inputs as well as for calculation of the input parameter, P_{wv}. In addition, aerosol optical properties are derived from AERONET (Aerosol Robotic Network) Level 2 data from Gosan in Jeju Island, covering the same period (Fig. 2).

The calculated P_{wv} values shown in Fig. 2(d) are derived from the following empirical formula, with Okulov *et al.*'s (2002) water vapor function and Gueymard's (1994) water vapor scale height function, using surface air temperature and relative humidity data:

$$P_{wv} = \int_{z_0}^{z} \rho_v(z)dz = 0.1H(z)\rho_v(z_0) \quad (8)$$

where $\rho_v(z)$ (g m^{-3}) is the water vapor density at height z above sea level (z_0), $H=\int_{z_0}^{z}\frac{\rho_v(z)}{\rho_v(z_0)}dz$, $\rho_v(z_0)=216.7\frac{RH(z_0)e_s(T_K)}{T_K}$ and $e_s(T_K)$ is the saturated vapor pressure at T_K, which equals T_{air}+273.15, as parameterized by Goff (1957). The water vapor scale height, H (km), was estimated from Gueymard (1994)'s empirical formula:

$$H = 0.4976 + 1.5265T_\theta + \exp(13.6897T_\theta - 14.9188T_\theta^3) \quad (9)$$

where $T_\theta = \frac{T_K}{273.15}$.

The spectral aerosol optical thickness $\tau_a(\lambda)$ is determined from the Ångström formula, including the Ångström exponent (α) and the turbidity coefficient (β), given as:

$$\tau_a(\lambda) = \beta\lambda^{-\alpha} \quad \text{with} \quad (10)$$

$$\beta = \tau_a(\lambda_0)\lambda_0^{\alpha}$$

where λ_0 is a reference wavelength. α can be calculated from a pair of aerosol optical thicknesses at any wavelengths (λ_1, λ_2) using the Volz method:

$$\alpha = \frac{\ln\left(\frac{\tau_a(\lambda_1)}{\tau_a(\lambda_2)}\right)}{\ln\left(\frac{\lambda_2}{\lambda_1}\right)} \quad (11)$$

The Level 2 (cloud-screened) α data of 440/870 nm for the ≤870 nm wavelengths and 675/870 nm for the >870 nm wavelengths are used to calculate the spectral aerosol optical thickness, following the method of Smirnov *et al.* (2003). In addition, the aerosol optical thickness at 440 nm wavelength, $\tau_a(\lambda_0$=440 nm), is used as a reference value in determining β.

Since the East China Sea is directly influenced by the East Asian monsoon climate, as shown in Fig. 2, meteorological factors reflect its seasonal variation: low summertime atmospheric pressure (mean 1002.5±2.4 hPa in August), high summertime relative humidity (mean 88.9±8.3% in June), precipitable water vapor (mean 4.6±0.4 cm in July and August) and a mean Ångström exponent of 1.57±0.31 in August. Interestingly, wind speed and its standard deviation are lowest in May (mean 2.6 m s^{-1}, standard deviation 0.5 m s^{-1}). The aerosol optical thickness at 440 nm exhibits high daily variation (>±0.09) through the entire year, tending towards low values in autumn (mean 0.18±0.12 in October).

For this study, 928 hr clear-sky data sets at the sea-surface are produced anew (Fig. 3) for conditions when the difference between the RTM irradiance and the IORS *in situ* data is <50 W m^{-2} and θ is <80°. These two limiting conditions used are to extract the clear sky irradiance data from in situ data and to avoid cosine response problems (Jacovides *et al.* 2003) with regard to analysis. When the

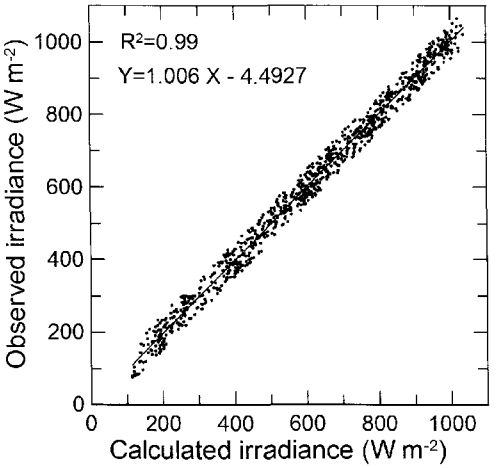

Fig. 3. Comparisons of hourly irradiance values from the RTM (200-4000 nm) with IORS observations (300-2800 nm) in 2004 under the conditions that their differences are <50 W m^{-2} and θ<80°.

RTM irradiance (200-4000 nm) is integrated at the measured spectral ranges (300-2800 nm), the value of the regression-line intercept (=-3.97) is slightly increased by 0.52 (not shown) with R^2=0.99 and slope=1.007 (not shown). It should be noted that the meteorological and atmospheric data used in calculating the selected clear-sky irradiance data are used for analysis and experiments.

4. Results and Discussion

Variability in PAR irradiance ratio to total irradiance

Fig. 4 shows that the ratio of PAR irradiance to total irradiance for cloudless-sky conditions just above the sea-surface varies seasonally from an average of 0.438 in January to 0.476 in July 2004. That is, the ratio is relatively higher during summer (>0.47) and lower during winter (<0.445), with slightly higher values occurring during autumn than during spring. The annual mean and standard deviation values are 0.461 and 0.017, respectively. In contrast, Jacovides *et al.* (2003) reported a slightly different pattern of seasonal variation for the eastern Mediterranean Sea: a minimum value of 0.421 in March and maximum value of 0.473 in June with an annual mean value of 0.454. Annual variability in the PAR irradiance ratio associated with changes in the atmospheric path length is explored with respect to diurnal cycles (Fig. 5(a)), and the solar zenith angle (Fig. 5(b)). Fig. 5(a) illustrates that throughout the entire year the PAR irradiance ratio is

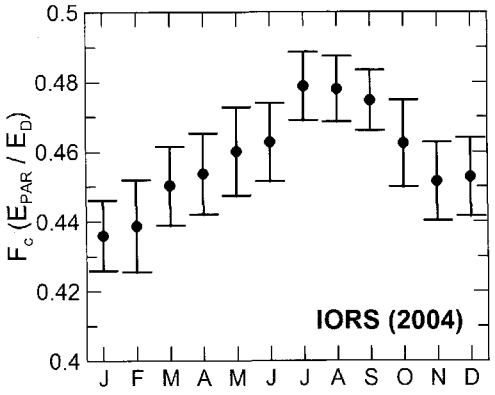

Fig. 4. Monthly variability in the simulated ratio (F_c) of PAR irradiance (E_{PAR}) to total irradiance (E_D) at the IORS in 2004 under clear sky conditions.

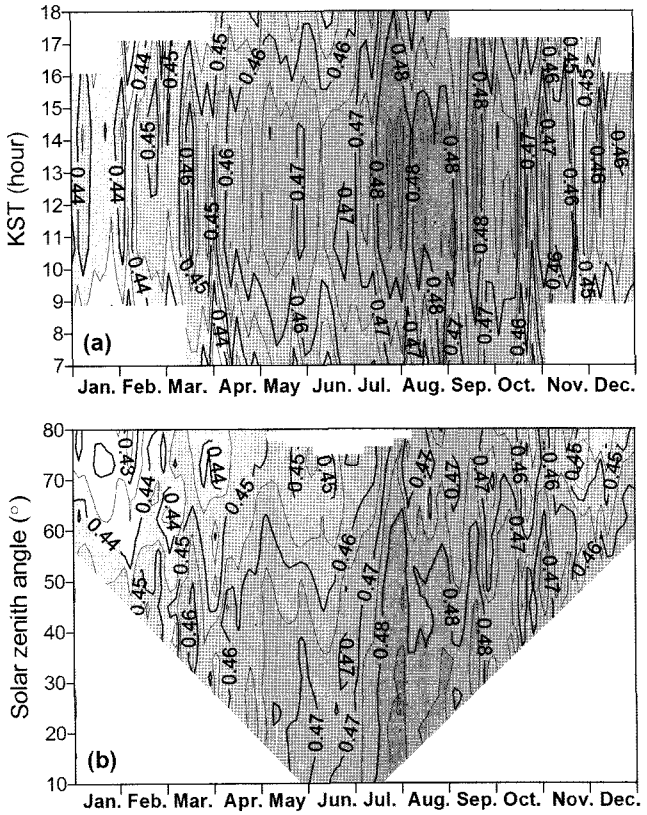

Fig. 5. Hourly variability in the simulated ratio (F_c) of PAR irradiance (E_{PAR}) to total irradiance (E_D) with respect to daytime (a) and solar zenith angle (b).

<0.02 lower during the two hours before sunset and sunrise relative to at midday; the ratio difference in summer is about 0.015 larger than that in winter. At a daily time scale, the ratios peak around noon.

Throughout the year the higher the solar zenith angle is, the lower the ratio is (Fig. 5(b)). This reduction likely

results from increasing atmospheric path lengths; notably PAR irradiance (*i.e.* 350-700 nm wavebands) is more sensitive than total irradiance (*i.e.* other wavebands) to this effect. These results conform to the findings of Baker and Frouin (1987), who used a maritime aerosol spectral model to show that the PAR irradiance ratio gradually decreases from θ=50°, and rapidly decreases from θ=60° (where the atmospheric path length is almost double).

Along with daily variability, our RTM results clearly show seasonal variability in the PAR irradiance ratio. The question as to which meteorological parameters produce this seasonal ratio variation is explored in next section.

The main factor contributing to seasonal variability in the PAR irradiance ratio

The input variables summarized in Table 1 affect the atmospheric transmittance of the direct and diffuse downwelling irradiances. Here we examine the sensitivity of PAR irradiance simulations to each input variable in order to discern the key variables affecting seasonal variability in the PAR irradiance ratio. Sensitivity tests were conducted on each input variable for two extreme cases: (1) using constant annual minimum and maximum input values and (2) using constant annual averaged values for the input variable (Table 2). The RTM simulation using the hourly meteorological and atmospheric data is referred to as the 'standard run' in this study.

The results of the sensitivity tests are compared to that of the standard run through the RMS (Root Mean Square) error. As shown in Table 2, the PAR irradiance ratio, F_c, is relatively sensitive to the following two parameters: precipitable water vapor content (~0.012-0.050 RMS errors) and aerosol optical thickness (~0.006-0.016 RMS errors). The PAR irradiance ratio is little affected by relative humidity and atmospheric pressure values. Notably, the P_{wv} RMS errors of E_D (16-76 W m^{-2}) are markedly larger than those of E_{PAR} (0.6-1.7 W m^{-2}). These results clearly indicate that most water vapor absorption occurs outside the 350-700 nm wavelengths, resulting in seasonal variation in the PAR irradiance ratio with changing seasonal water vapor content in temperate monsoon-climate oceanic regimes (see Fig. 2(d)). Similarly, Jacovides *et al.* (2003) pointed out that an increase in water-vapor content during September is conducive to high PAR irradiance ratios in the eastern Mediterranean Sea. According to Baker and Frouin (1987), the year-round high levels of atmospheric-water vapor are the main reason why PAR irradiance ratios are higher in the tropics than in the mid- and high-latitudes.

Fig. 6 supports the idea that the PAR irradiance ratio is strongly correlated to total-precipitable water vapor (R^2=

Table 2. Comparisons of the calculated F_c, E_D, E_{PAR}, E_{DD} and E_{DS} between the standard run and experiments using minimum, maximum and mean values of each variable.

Variable		RMS error				
		F_c	E_D (W m^{-2})	E_{PAR} (W m^{-2})	E_{DD}^{*} (W m^{-2})	E_{DS}^{**} (W m^{-2})
P_{wv} (cm)	Min. : 0.11	0.050	76.5	1.7	67.1	13.4
	Max.: 5.11	0.021	27.2	1.1	21.9	6.2
	Mean: 2.55	0.012	16.4	0.6	13.6	3.4
τ_a (440 nm)	Min. : 0.00	0.016	40.4	26.0	186.7	148.9
	Max.: 2.20	0.016	71.8	41.9	331.5	263.0
	Mean: 0.37	0.006	16.1	10.3	79.4	64.3
α (α$_1$, α$_2$)***	Min. : 0.00, 0.00	0.007	4.2	4.3	83.8	86.4
	Max.: 2.23, 2.66	0.006	7.8	1.9	63.2	57.1
	Mean: 1.11, 1.02	0.003	2.3	1.5	24.6	25.0
RH (%)	Min. : 30	0.0012	3.9	2.2	-	3.9
	Max.: 100	0.0008	2.0	1.2	-	2.0
	Mean: 70	0.0053	1.4	0.8	-	1.4
A_p (hPa)	Min. : 990	0.0007	0.9	0.7	1.0	0.3
	Max.: 1030	0.0007	0.9	0.7	1.1	0.3
	Mean: 1012	0.0004	0.3	0.2	0.4	0.1

*$E_{DD} = \int_{200}^{4000} E_{dd}(\lambda)d\lambda$, **$E_{DS} = \int_{200}^{4000} E_{ds}(\lambda)d\lambda$ and α$_1$ and α$_2$ in ***α(α$_1$, α$_2$) are aerosol Ångström exponent data of 440/870 nm for 870 nm wavelength and of 675/870 nm for >870 nm wavelength, respectively.

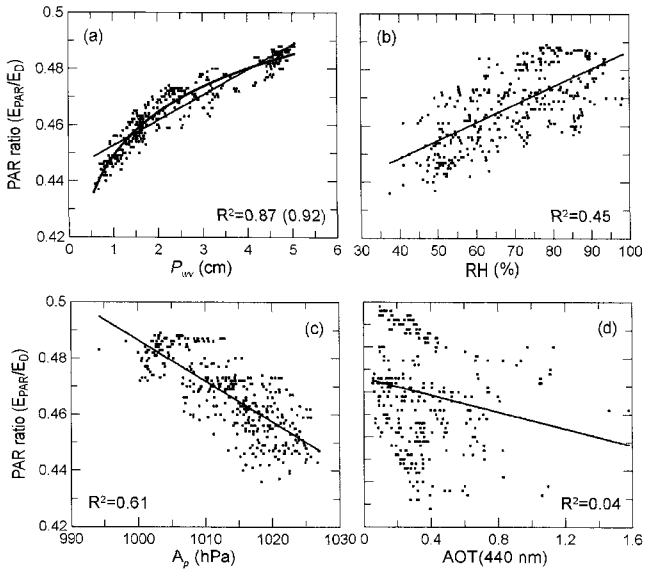

Fig. 6. Relationships between the simulated ratio (F_c) of PAR irradiance (E_{PAR}) to total irradiance (E_D) and the main RTM input variables.

0.87 for linear regression and R^2=0.91 for logarithmic regression), but has relatively-weak correlations with atmospheric pressure (R^2=0.61) and relative humidity (R^2=0.45), and no correlation with aerosol optical thickness (R^2=0.04). Since the τ_a RMS errors for E_D and E_{PAR} are of the same order of magnitude (16-72 W m^{-2} for E_D and 10-42 W m^{-2} for E_{PAR}) as shown in Table 2, aerosol optical thickness is likely to significantly influence the entire spectrum, leading to poor correlation with the PAR ratio variation. Also this is the most sensitive parameter affecting both direct and diffuse downwelling irradiances. It should be noted that clear-sky data for θ<60° (*i.e.* hours 11, 12, 13 and 14 in Korean Standard Time) were used for the above analyses in order to minimize the effect of atmospheric path length on the PAR irradiance ratio.

According to Kim *et al.* (2002), aerosol optical thickness in the East China Sea is significantly influenced by Asian dust (mineral aerosol) blown from the Chinese and Mongolian deserts and anthropogenic aerosols transported from the eastern industrial area of China during spring.

Additional sensitivity tests were conducted for each input variable using monthly-averaged values in order to explore their sensitivity to seasonal meteorological and atmospheric conditions. The RTM simulations were also conducted with monthly-averaged values and annual-averaged values for all parameters. Table 3 shows that the RMS errors for each monthly-averaged test are one order of magnitude lower than those in the previous sensitivity tests for each variable (*i.e.* the two extreme cases and each annual-averaged parameter case). Even though the RMS errors of all variables are significantly reduced, the τ_a RMS errors for direct and diffuse downwelling irradiances are still large (>50 W m^{-2}). These results reveal that use of monthly-averaged meteorological and atmospheric values can produce reasonable PAR irradiance ratio, E_{PAR}, and E_D results. However, under atmospheric conditions with large short- and long-term changes in aerosol optical thickness, use of τ_a values reflecting this rapid variation is required to obtain more accurate E_{DD} ($\int_{200}^{4000} E_{dd}(\lambda)d\lambda$) and E_{DS} ($\int_{200}^{4000} E_{ds}(\lambda)d\lambda$) results.

PAR irradiance ratio variation from just above to just below the sea-surface

In previous sections we investigated the peculiarities of daily and monthly variations in the PAR irradiance ratio just above the sea-surface under clear-sky conditions. In this section, we examine PAR irradiance ratio variation from just above to just below the sea surface caused by sea-surface reflection effects.

Fig. 7(a) shows that changes in the PAR irradiance ratio

Table 3. Comparisons of the calculated F_c, E_D, E_{PAR}, E_{DD} and E_{DS} values between the standard run and experiments using monthly-averaged values for each input variable and monthly- averaged (M_{all}) and annual-averaged (A_{all}) values for all input values.

Variable	RMS error				
	F_c	E_D (W m^{-2})	E_{PAR} (W m^{-2})	E_{DD} (W m^{-2})	E_{DS} (W m^{-2})
P_{wv} (cm)	0.0045	6.1	0.2	5.1	1.3
τ_a (440 nm)	0.0042	12.4	7.9	65.0	53.4
α (α_1, α_2)	0.0018	1.8	1.2	19.5	19.9
RH (%)	0.0004	0.9	0.5	0.0	0.9
A_p (hPa)	0.0003	0.2	0.1	0.2	0.1
M_{all}	0.0064	13.8	7.8	71.0	59.7
A_{all}	0.0126	22.3	10.1	87.4	74.2

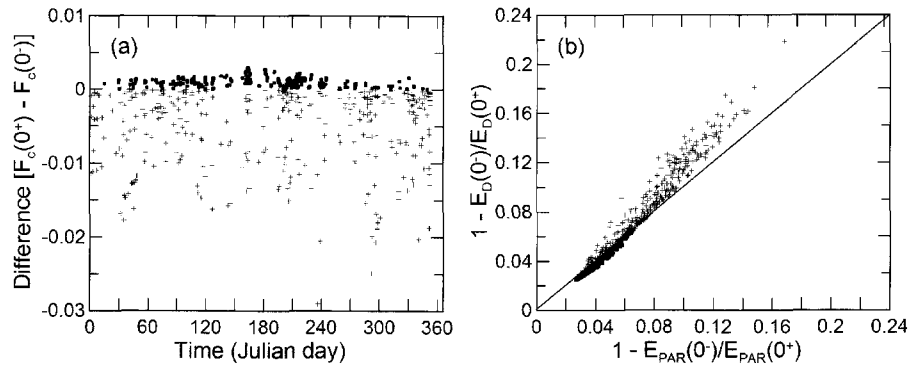

Fig. 7. (a) PAR irradiance ratio differences between just above and just below the sea surface and (b) the relationship between the rate of change of E_D and that of E_{PAR} at the sea-surface. Dots denote $F_c(0^+) > F_c(0^-)$ and vice versa for crosses.

($F_c(0^+)$–$F_c(0^-)$) from just above to just below the sea surface induced by the sea-surface reflectivity range from -0.03~0.003. Variation in the negative values (*i.e.* the case of $F_c(0^+) < F_c(0^-)$) is one order of magnitude higher than that of the positive values, indicating that the decreases in the PAR irradiance ratio (*i.e.* the case of $F_c(0^+)>F_c(0^-)$) induced by surface conditions are relatively small. When the rate of change in $E_{PAR}(0^+)$ is greater than that of change in $E_D(0^+)$, the PAR irradiance ratio difference is positive, and vice versa (Fig. 7a, b). Reflections of $E_D(0^+)$ and $E_{PAR}(0^+)$ at the sea-surface are roughly less than 0.16.

As shown in Fig. 8, after reflection the PAR irradiance ratio just below the sea-surface tends to increase by an average of 0.012 (±0.005) with high solar zenith angles (>60°) and strong wind speeds (>8 m s^{-1}), and vice versa. Vigorous wind conditions actively generate sea foam and bubbles somewhat below the sea-surface. Under these conditions, foam reflectance (R_f) becomes important: the near-IR wavelengths are more strongly absorbed pre-seawater reflection than the visible wavelengths, leading to PAR irradiance ratio increases. In addition, under θ>60° conditions without vigorous wind, the near-IR wavelengths are more strongly reflected than the visible wavelengths, resulting in PAR irradiance ratio increases.

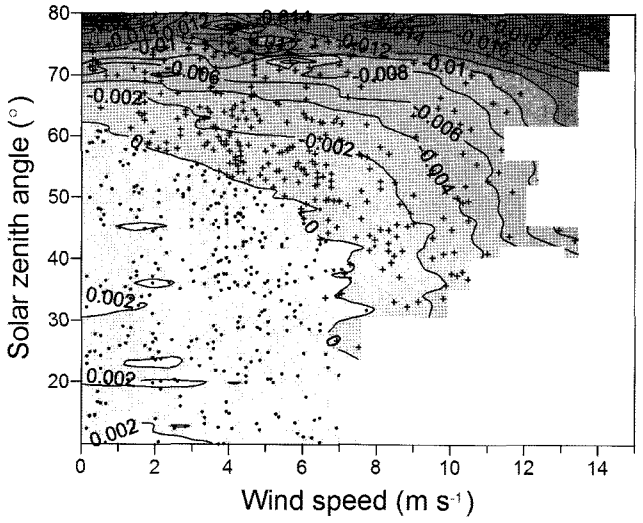

Fig. 8. Relationship between PAR irradiance ratio changes from just above to just below the sea-surface and wind speed and solar zenith angle. Dots denote $F_c(0^+)>F_c(0^-)$ and vice versa for crosses.

5. Conclusion

Through a simple clear-sky radiative transfer model, we examined temporal variation in the ratio of PAR irradiance to total irradiance and key associated parameters at the Ieodo Ocean Research Station in the East China Sea. The preliminary results show that the PAR irradiance ratio varies seasonally from an average of 0.44 (±0.01) in January to an average of 0.48 (±0.01) in July 2004, with average daily variations at these times of 0.016 (±0.008) and 0.025 (±0.008), respectively. The PAR irradiance ratio is mainly controlled by the following three key factors: daily and seasonal change in the solar zenith angle, seasonal variability in precipitable water vapor, and daily and seasonal variability in aerosol optical thickness. Since the East China Sea is characterized by the East Asian monsoon climate, seasonal variation in atmospheric conditions significantly affects seasonal variation in PAR in this region. In addition, increases in reflectance due to strong wind stress (>8 m s^{-1}) and high solar zenith angles (>60°) lead to average increases of 0.012 (±0.005) in the PAR irradiance ratio just below the sea-surface. Model

sensitivity tests demonstrate that use of accurate input data for the two key variables of precipitable water vapor and aerosol optical thickness is necessary for accurate PAR simulations.

In conclusion, our ultimate aim is to parameterize vertical spectral PAR attenuation (absorption and scattering) in the East China Sea, depending on water itself, phytoplankton, detritus and other substances. This work constitutes the first step towards developing an appropriate PAR parameterization for use in modeling the ecosystem of the East China Sea. The next step will be to consider cloud effects and to compare the calculated values with the observed irradiance and PAR. Systematic and comprehensive observations of atmospheric factors are, thus, also needed.

Acknowledgments

We would like to thank the Dr. D. Hart at the University of Canterbury for helpful comments and a reviewer, Dr. Hyoun-Woo Kang for the constructive and helpful comments which have significantly improved this work.

References

Baker, K.S. and R. Frouin. 1987. Relation between photosynthetically available radiation and total insolation at the ocean surface under clear skies. *Limnol. Oceanogr.*, **32**, 1370-1377.

Baretta-Bekker, J.G., J.W. Baretta, and W. Ebenhöh. 1997. Microbial dynamics in the marine ecosystem model ERSEM II with decoupled carbon assimilation and nutrient uptake. *J. Sea Res.*, **38**, 195-211.

Byun, D.-S., X.H. Wang, M. Zavatarelli, and Y.-K. Cho. 2006. Effects of resuspended sediments and vertical mixing on phytoplankton spring bloom dynamics in a tidal estuarine embayment. *J. Mar. Syst.* (in press).

Byun, D.-S., X.H. Wang, D.E. Hart, and Y.-K. Cho. 2005. Modeling the effect of freshwater inflows on the development of spring blooms in an estuarine embayment. *Estuar. Coast. Shelf Sci.*, **65**, 351-360.

Colijn, F.G. and C. Cadée. 2003. Is phytoplankton growth in the Wadden Sea light or nitrogen limited? *J. Sea Res.*, **49**, 83-93.

Ebenhöh, W., J.G. Baretta-Bekker, and J.W. Baretta.1997. The primary production module in the marine ecosystem model ERSEM II, with emphasis on the light forcing. *J. Sea Res.*, **38**, 173-193.

Goff, J.A. 1957. Saturation pressure of water on the new Kelvin temperature scale, Transactions of the American Society of Heating and Ventilating Engineers. p. 347-354. In: *The semi-annual meeting of the American society of heating and ventilating engineers,* Murray Bay, Quebec, Canada.

Gregg, W.W. and K.L. Carder. 1990. A simple spectral solar irradiance model for cloudless maritime atmospheres. *Limnol. Oceanogr.*, **35**, 1657-1675.

Gregg, W.W. 2002. A coupled ocean-atmosphere radiative model for global ocean biogeochemical models. Technical report series on global modeling and data assimilation 22. ed. by M. Suarez. NASA/TM---2002-104606. 19 p.

Gueymard, C. 1994. Analysis of monthly average atmospheric precipitable water and turbidity in Canada and Northern United States. *Sol. Energy*, **53**, 57-71.

Gueymard, C. 2001. Parameterized transmittance model for direct beam and circumsolar spectral irradiance. *Sol. Energy*, **71**, 325-346.

Jacovides, C.P., F.S. Tymvios, D.N. Asimakopoulos, K.M. Theofilou, and S. Pashiardes. 2003. Global photosynthetically active radiation and its relationship with global solar radiation in the Eastern Mediterranean basin. *Theor. Appl. Climatol.*, **74**, 227-233.

Jitts, H.R., A. Morel, and Y. Saijo. 1976. The relation of oceanic primary production to available photosynthetic irradiance. *J. Mar. Freshwater Res.*, **27**, 441-454.

Justus, C.G. and M.V. Paris. 1985. A model for solar spectral irradiance and radiance at the bottom and top of a cloudless atmosphere. *J. Climat. Appl. Meteor.*, **24**, 193-205.

Kasten, F. and A.T. Young. 1989. Revised optical air mass tables and approximation formula. *Appl. Opt.*, **28**, 4735.

Kim, J.-Y., B.-C. Choi, and S.-N. Oh. 2002. Spectral aerosol optical depth of Asian dust measured by sunphotometer at Kosan during ACE-Asia. *J. Korean Meteorol.*, **38**, 355-367. (In Korean)

Koepke, P. 1984. Effective reflectance of oceanic whitecaps. *Appl. Opt.*, **23**, 1816-1824.

Knauss, J.A. 1997. The transfer of heat across the ocean surface. p. 39-58. In *Introduction to physical oceanography.* Prentice-Hall.

Morel, A. and R.C. Smith. 1974. Relation between total quanta and total energy for aquatic photosynthesis. *Limnol. Oceanogr.*, **9**, 591-600.

Morel, A. 1988. Optical modeling of the upper ocean in relation to its biogenous matter content (Case I waters). *J. Geophys. Res.*, **93**, 10,749-10,768.

Okulov, O., H. Ohvril, and R. Kivi. 2002. Atmospheric precipitable water in Estonia, 1990-2001. *Bor. Environ. Res.*, **7**, 291-300.

Paltridge, G.W. and C.M.R. Platt. 1976. Radiative Processes in Meteorology and Climatology. Elsevier, Amsterdam. 318 p.

Parsons, T.R., M. Takahashi, and B. Hargrave. 1984. Biological oceanographic processes. Pergamon Press, Oxford. 330 p.

Shim, J.S, I.S. Chun, and I.K. Min. 2004. Construction of Ieodo Ocean Research Station and its operation. *Int. Soc. Offshore*

Polar Eng., 2004, **13**, 1-7.

Smirnov, A, B.N. Holben, O. Dubovik, R. Frouin, T.F. Eck, and I. Slutsker. 2003. Maritime component in aerosol optical models derived from Aerosol Robotic Network data. *J. Geophys. Res.*, **108**, D1, 4033, doi:10.1029/2002JC002701.

Stramska, M. and T. Petelski. 2003. Observations of oceanic whitecaps in the north polar waters of the Atlantic. *J. Geophys. Res.*, **108**, C3, 3086, doi:10.1029/2002JC001321.

Tilzer, M.M. and C.R. Goldman. 1978. Importance of mixing, thermal stratification and light adaptation for phytoplankton productivity in Lake Tahoe (California-Nevada). *Ecology*, **59**, 810-821.

Van Heuklon, T. K. 1979. Estimating atmospheric ozone for solar radiation models. *Sol. Energy*, **22**, 63-68.

Zavatarelli, M., J.W. Baretta, J.G. Baretta-Bekker, and N. Pinardi. 2000. The dynamics of the Adriatic Sea ecosystem: An idealized model study. *Deep-Sea Res. Part I*, **47**, 937-970.